ISOMAse
International Society of Ocean, Mechanical and Aerospace Scientists and Engineers
Journal of Ocean, Mechanical and Aerospace
-Science and Engineering-
30 March 2026. Vol.70 No.1
DOI: 10.36842/jomase.v70i1.632

The Effect of U-Bends on the Convective Heat Transfer Coefficient of Nanofluids Flow

Alamirsyah[a] and Adek Tasri[a*]

[a)]Department of Mechanical Engineering, Andalas University, Padang, West Sumatra, Indonesia

*Corresponding author: adek.tasri@eng.unand.ac.id

Paper History

Received: 20-March-2026
Received in revised form: 27-March-2026
Accepted: 30-March-2026

ABSTRACT

One effort that can increase the convection heat transfer coefficient between fluid and solid surface is adding nanoparticles to the fluid. However, there are several flow-path conditions, such as concavities and U-turns, can affect the distribution of nanoparticles in the fluid and, in turn, the heat transfer coefficient. This paper studies the effect of a U-turn on the transfer coefficient. The study was conducted using numerical simulations to determine changes in the heat transfer coefficient along the U-turn. It was found that the convection heat transfer coefficient increased at several locations on the outside of the U-turn. The heat transfer coefficient also increased at several locations on the inside of the bend, though by smaller amounts.

KEYWORDS: *Nanofluids, Reynolds Number, U-bend, Heat Transfer Coefficient, CFD,* Al_2O_3.

NOMENCLATURE

Dh	Hydraulic diameter
De	Dean number
DPM	Discrete Phase Model
FB	Brownian force
FD	Drag force
FG	Gravitational force
FL	Saffman lift force
FP	Pressure gradient force
FT	Thermophoresis force
FV	Virtual mass force
Gk, Gω	Production terms for k and ω
mp	Particle mass
Pr	Prandtl number
U	Characteristic velocity
up	Particle velocity
Yk, Yω	Turbulent dissipation terms for k and ω
Γk, Γω	Effective diffusivities for k and ω
φ	Nanoparticle volume fraction
ν	Kinematic viscosity
ω	Specific dissipation rate
κ	Radius of curvature of the bend
dp	Nanoparticle diameter

1. INTRODUCTION

Thermal management and heat exchange efficiency remain critical concerns across engineering applications, ranging from automotive cooling and HVAC systems to power generation and electronic cooling. As industrial systems become increasingly compact and power-dense, the demand for high-performance heat transfer fluids and optimized flow geometries continues to grow. The efficiency of a heat exchanger is largely governed by the convective heat transfer coefficient (h) of the working fluid and the hydrodynamic characteristics of its flow path [1-5]. Conventional coolants such as water, ethylene glycol, and engine oil possess inherently low thermal conductivity, which limits heat dissipation rates in compact systems [6-10]. Nanofluids have emerged as a promising alternative; for instance, certain nanofluids in double-pipe U-bend configurations have achieved a 14.76% higher Nusselt number than water under comparable industrial flow conditions [6].

Among candidate nanoparticle materials, aluminum oxide (Al_2O_3) was selected for this study due to its chemical stability, cost-effectiveness relative to metallic nanoparticles, and extensive documentation in the literature. Pak and Cho reported a convective heat transfer coefficient enhancement of approximately 45% for γ-Al_2O_3-water nanofluid at a volume fraction of 1.34% [11], a concentration adopted here for model validation to balance heat transfer enhancement against pumping penalty.

Beyond fluid properties, flow geometry plays an equally important role in heat transfer performance. Piping systems frequently incorporate U-bends to accommodate spatial constraints, and flow through a 180° U-bend exhibits

ISOMAse International Society of Ocean, Mechanical and Aerospace Scientists and Engineers
Journal of Ocean, Mechanical and Aerospace
-Science and Engineering-
30 March 2026. Vol.70 No.1
DOI: 10.36842/jomase.v70i1.632

hydrodynamic behavior markedly different from straight-pipe flow [12]. Curvature-induced centrifugal forces generate secondary Dean vortices that disrupt the thermal boundary layer and enhance convective heat transfer, at the cost of increased pressure drop [13]. At high Reynolds numbers, this interaction between centrifugal migration and turbulent mixing becomes especially pronounced: nanoparticle concentration near the outer wall intensifies, turbulent boundary layers thin, and the four mechanisms known to enhance nanofluid heat transfer increased effective thermal conductivity, Brownian motion, changes in fluid viscosity and boundary layer thickness, and particle–fluid interaction no longer act uniformly around the pipe circumference [14-15].

Despite growing research on nanofluids and on U-bend flows separately, limited data exist on how these enhancement mechanisms redistribute circumferentially within a U-bend at high Reynolds number, where centrifugal and turbulent effects are strongest. Characterizing this regime is essential for the design of compact U-bend heat exchangers operating near their thermal-hydraulic limits.

This study therefore investigates the convective heat transfer coefficient of Al_2O_3/water nanofluid (φ = 1.34%) flowing through a 180° U-bend at Re = 100,000, using ANSYS Fluent with a two-phase Euler–Lagrange (DPM) framework and the SST k-ω turbulence model, validated against the Dittus–Boelter and Pak and Cho (1998) correlations to within 10% deviation [11], [16-17]. The results are used to identify how the U-bend geometry redistributes heat transfer enhancement around the outer, inner, and side walls at this high-Re condition, providing design-relevant insight beyond what Reynolds number alone can explain [18], [19].

2. METHOD

This study employs a numerical approach to investigate the effect of a 180° U-bend pipe geometry on the convective heat transfer coefficient of Al_2O_3/water nanofluid at Re = 100,000. The analysis is conducted entirely through Computational Fluid Dynamics (CFD) simulation using ANSYS Fluent, utilizing a two-phase Euler–Lagrange (Discrete Phase Model, DPM) framework to resolve the turbulent flow and nanoparticle transport within the bend. The U-bend pipe geometry specification is depicted in Table 1 and the U-turn geometry shows in Figure 1.

2.1 Modelling

The computational domain was generated using ANSYS Design Modeler. Two geometries were built: a straight pipe (D = 10.66 mm, L = 3,520 mm) used for CFD solver validation, and a 180° U-bend pipe (D = 10 mm) used as the primary test section. A hydrodynamic entry length of 350 mm — calculated for the highest Reynolds number tested (Re = 100,000) using:

$$Lh = 4,4 \cdot Re^{1/6} \cdot D \tag{1}$$

Table 1: U-bend pipe geometry specification

D (mm)	Length (mm)	R1 (mm)	R2 (mm)
10	100	10	20

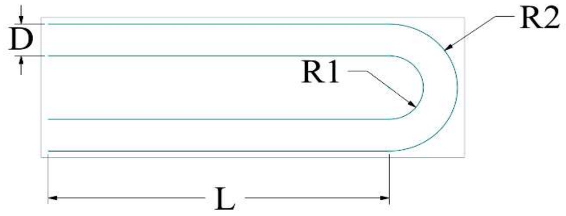

Figure 1: The U-turn geometry

L_h = 4.4·Re^(1/6)·D plus a 50 mm safety margin was applied uniformly to both geometries to ensure fully developed inlet flow. A dominant hexahedral meshing strategy was adopted, with the fluid cross-section partitioned into an O-grid structure (a central rectangular core surrounded by four outer curved blocks) to resolve nanoparticle migration through the bend water (H_2O) was used as the continuous base fluid, and Al_2O_3 nanoparticles (d_p = 13 nm, φ = 1.34%) as the discrete phase, with properties summarized in Table 2.

Table 2: Nanofluid properties

Property	Symbol	Water (H_2O)	Al_2O_3	Unit
Density	ρ	998.2	3880	kg/m³
Dynamic Viscosity	μ	0.001262	—	kg/m·s
Thermal Conductivity	k	0.600	36	W/m·K
Specific Heat Capacity	C_p	4.182	0.773	kJ/kg·K
Particle Diameter	D_p	—	13	nm

2.2 Governing Equation

In this simulation, the conservation equations are solved for the fluid phase as a continuous phase, including the continuity, momentum, and energy equations expressed in Equations (2) through (4) below:

Continuity Equation:

$$\nabla\cdot\left(\rho_f\bar{u}\right)=0 \tag{2}$$

Momentum Equation:

$$\nabla\cdot\left(\rho_f\bar{u}\bar{u}\right) = -\nabla_p + \nabla\cdot\tau \tag{3}$$

Energy Equation:

$$\nabla\cdot\left(\rho_f\bar{u}C_{p\cdot f}T\right) = \nabla\cdot\left(k_f\nabla T - C_{p\cdot f}\rho_f\overline{ut}\right) \tag{4}$$

For turbulence modeling, the SST K−ω model is used, which is capable of providing accurate predictions in both the near-wall and free-stream regions. This model solves two transport equations: the turbulent kinetic energy (k) and the specific dissipation rate (ω). The transport equation for k is given by the following equation:

$$\frac{\partial}{\partial t}(\rho k)+\frac{\partial}{\partial x_i}(\rho k u_i)=\frac{\partial}{\partial x_j}\left(\Gamma_k\frac{\partial k}{\partial x_j}\right)+G_k-Y_k+S_k+G_b \tag{5}$$

JOMAse | Received: 20 March 2026 | Accepted: 30-March-2026 | [(70) 1: 100-107]
Published by International Society of Ocean, Mechanical and Aerospace Scientists and Engineers, www.isomase.org., ISSN: 2354-7065 & e-ISSN: 2527-6085

ISOMAse
International Society of Ocean, Mechanical and Aerospace Scientists and Engineers
Journal of Ocean, Mechanical and Aerospace
-Science and Engineering-
30 March 2026. Vol.70 No.1
DOI: 10.36842/jomase.v70i1.632

Hence, the transport equation for ω is given by the following equation:

$$\frac{\partial}{\partial t}(\rho\omega) + \frac{\partial}{\partial x_i}(\rho\omega u_i) = \frac{\partial}{\partial x_j}\left(\Gamma_\omega \frac{\partial\omega}{\partial x_j}\right) + G_\omega - Y_\omega + S_\omega + G_{\omega b} \quad (6)$$

Where G_k and G_ω are the production terms for k and ω, Γ_k and Γ_ω are the effective diffusivities, and Y_k dan Y_ω are the turbulent dissipation terms for k and ω.

2.3 Discrete Phase Model (DPM) Equation

To model the motion of Al_2O_3 nanoparticles, an Euler-Lagrange-based DPM approach was used, in which the host medium is treated as the continuous phase and the nanoparticles as the discrete phase. The trajectory of each particle was tracked individually using the following equation of motion (7).

$$m_p \frac{d\vec{u}_p}{dt} = \vec{F_B} + \vec{F_T} + \vec{F_G} + \vec{F_V} + \vec{F_D} + \vec{F_P} + \vec{F_L} \quad (7)$$

where the right-hand side represents the resultant force acting on the particle, which includes the Brownian force (F_B), the thermophoresis force (F_T), the gravitational force (F_G), the virtual mass force (F_V), the drag force (F_D),), the pressure gradient force (F_P), and the Saffman lift force (F_L).

2.4 Validation

The CFD model was validated against the empirical correlation of Pak and Cho (1998) [11] using a straight pipe geometry (D = 10.66 mm, L = 3,520 mm) with Al_2O_3/water nanofluid at φ = 1.34%, focusing on Re = 100,000. The Nusselt number is defined as:

$$Nu = \frac{hD_h}{k} \quad (8)$$

and compared against the Pak and Cho (1998) correlation [11]:

$$Nu = 0.021Re^{0.8}\mathrm{Pr}^{0.5} \quad (9)$$

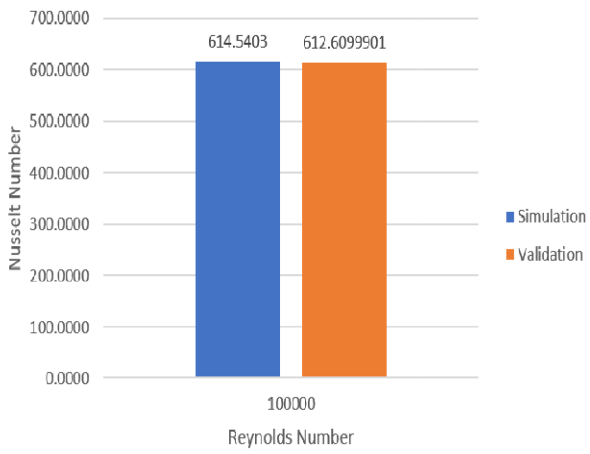

Figure 2: Validation graph

At Re = 100,000, the simulated Nusselt number for the straight pipe agreed with the empirical correlation within a deviation of less than 10%, satisfying the validation criterion. This confirms that the mesh resolution, SST k-ω turbulence settings, boundary conditions, and DPM coupling are correctly configured to capture convective heat transfer in turbulent nanofluid flow. The U-bend configuration at the same Reynolds number yielded a higher Nu than the straight pipe, attributed to Dean vortex-induced mixing, thereby establishing a validated baseline for assessing bend-induced heat transfer enhancement. In Figure 2 shows the validation graph.

3. RESULT AND DISCUSSION

The following section presents and discusses the heat transfer characteristics of Al_2O_3/water nanofluid flow through the 180° U-bend pipe across the five simulated Reynolds numbers. Heat transfer coefficient data were extracted along four axial lines (upper, lower, right, and left walls), enabling a comprehensive spatial characterization of the convective heat transfer distribution. Figure 3 provides an overview of the locations of these four extraction lines (A-A', B-B', C-C', D-D').

3.1 Heat Transfer Coefficient Along U-Bend

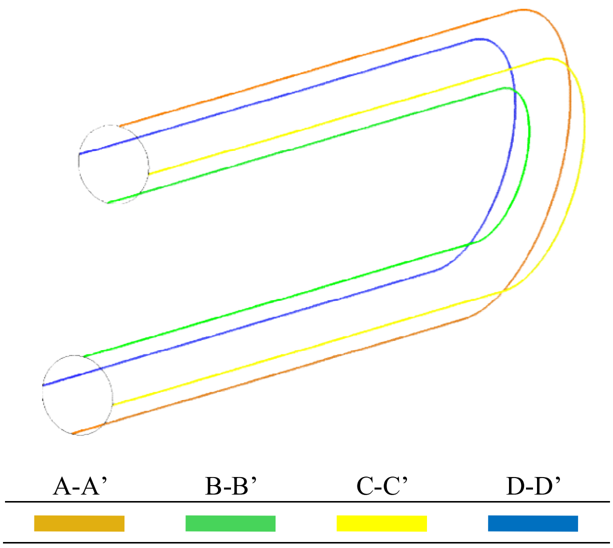

Figure 3: Location line along the u-bend pipe

At the Reynolds number 100,000 simulated, the contour (Figure 4 and the accompanying legend) spans the full range from 37680 to 257100 W/m²·K, and the value referenced elsewhere in the report as the peak mid-bend heat transfer coefficient. The outer wall of the bend is now sharply defined and clearly the dominant thermal feature of the geometry. In Figure 5, also shows the DPM concentration contour reaching 561 kg/m³ the highest particle concentration recorded across all five cases confirming that nanoparticle migration toward the outer wall continues to intensify up to the top of the Reynolds number range studied. Figures 6-7 show the velocity field peaking at roughly 18.5–20.7 m/s, with the

JOMAse | Received: 20 March 2026 | Accepted: 30-March-2026 | [(70) 1: 100-107]
Published by International Society of Ocean, Mechanical and Aerospace Scientists and Engineers, www.isomase.org., ISSN: 2354-7065 & e-ISSN: 2527-6085

streamlines showing the tightest, most sharply curved deflection around the bend of any case presented. The heat transfer coefficient value on each line location is provided in Table 3.

The four line graphs (Figure 8) show the widest spread of the entire subsection: Line A-A' peaks at 194601.906 W/m²·K, compared with 102495.18 W/m²·K on Line B-B' and 76779.9453 - 80580.1563 W/m²·K on Lines C-C' and D-D'. This is the clearest numerical demonstration in the report that the outer-wall enhancement effect does not merely persist but widens substantially in relative terms as Reynolds number increases.

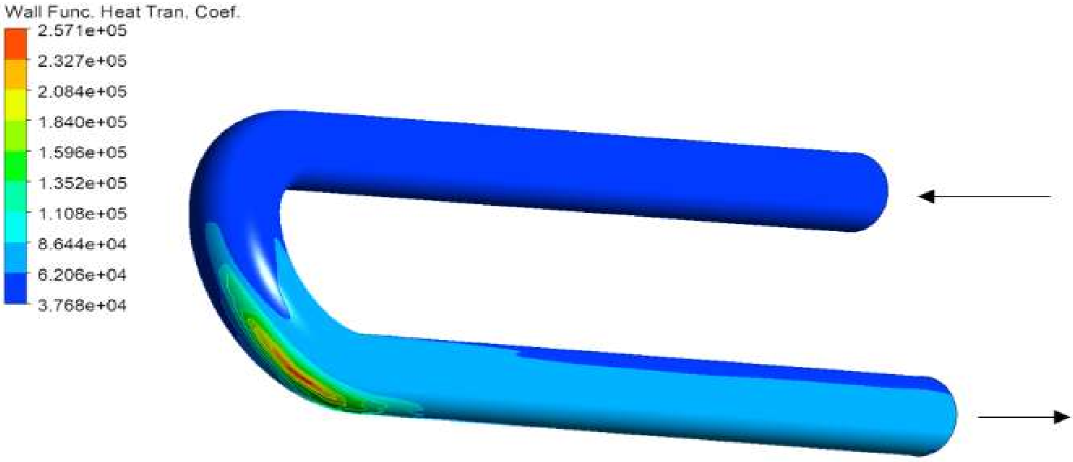

Figure 4: Heat transfer coefficient contour along u-bend pipe

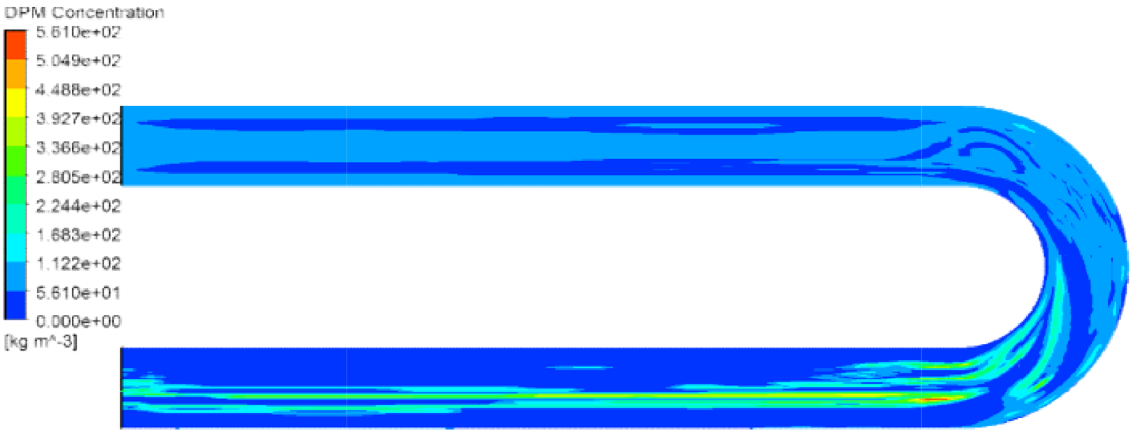

Figure 5: DPM concentration along u-bend pipe

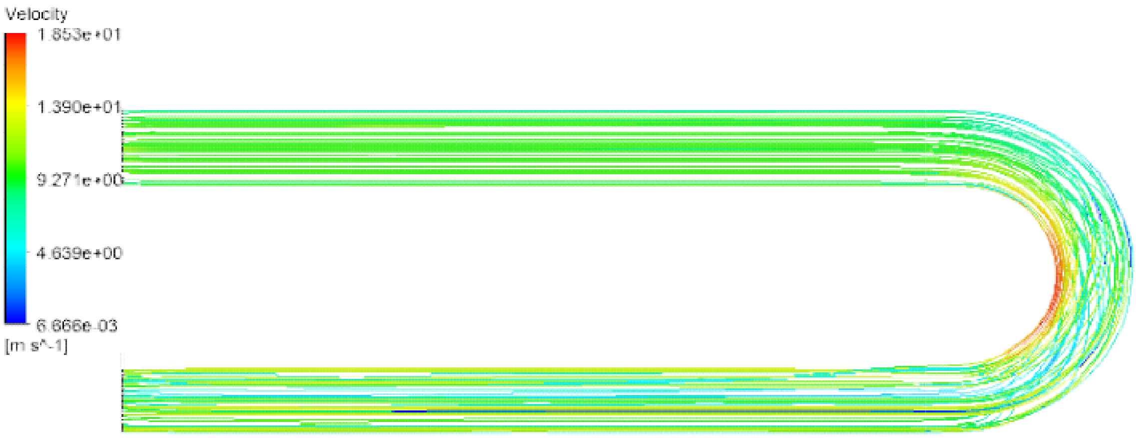

Figure 6: Velocity streamline along the u-bend pipe

JOMAse | Received: 20 March 2026 | Accepted: 30-March-2026 | [(70) 1: 100-107]
Published by International Society of Ocean, Mechanical and Aerospace Scientists and Engineers, www.isomase.org., ISSN: 2354-7065 & e-ISSN: 2527-6085

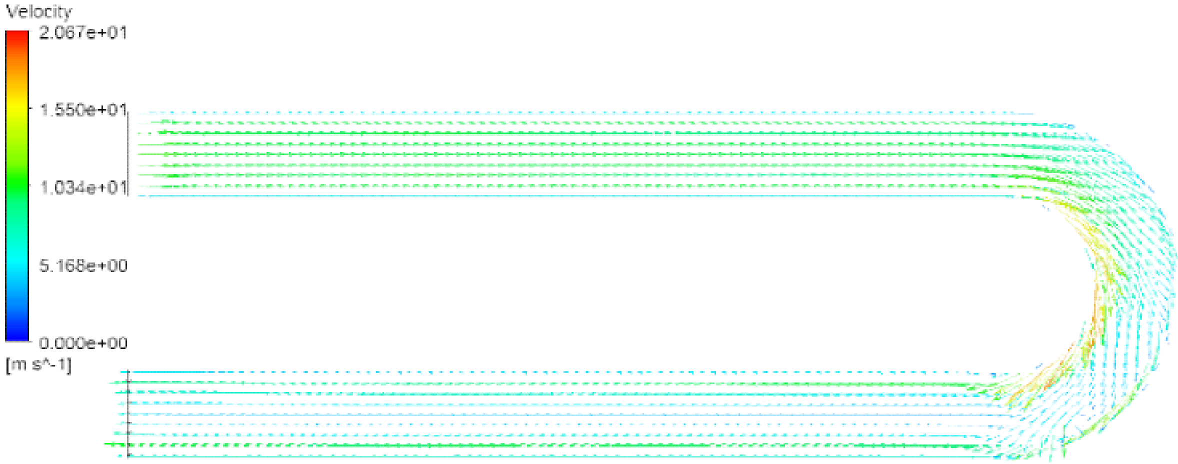

Figure 7: Velocity vector along u-bend pipe

Table 3: Heat transfer coefficient value on each line location

Line	Heat Tranfer Coefficient	
	Max	Min
A-A’	194601.9	40017.51
B-B’	102495.2	40041.25
C-C’	76779.95	40013.15
D-D’	80580.16	40139.59

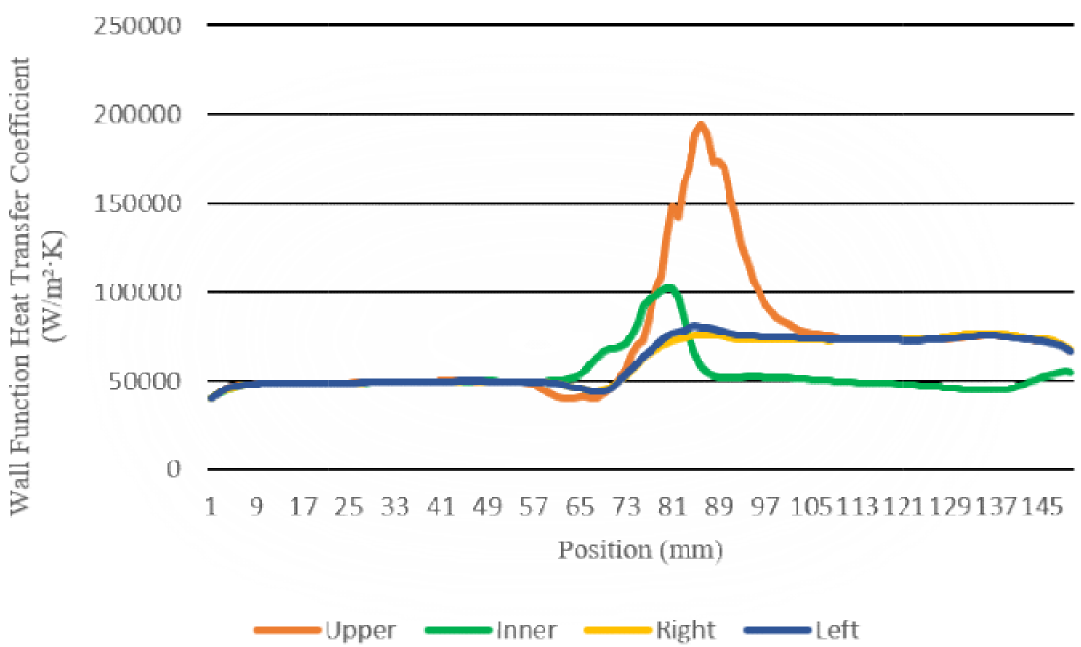

Figure 8: Heat transfer coefficient along u-bend pipe for each line

ISOMAse
International Society of Ocean, Mechanical and Aerospace Scientists and Engineers
Journal of Ocean, Mechanical and Aerospace
-Science and Engineering-
30 March 2026. Vol.70 No.1
DOI:
10.36842/jomase.v70i1.632

3.2 The Area with the Highest Heat Transfer Coefficient

Figure 9 provides the critical-area zoom for this case, and Figure 10 shows the corresponding pressure trace, which stays close to zero through most of the domain, dips briefly negative near chart counts 85, and then rises steeply to 8.47E+07, but reaching a lower absolute peak, which is consistent with a highly localized numerical artifact at the area rather than a physically meaningful bulk pressure rise. Temperature and DPM concentration monitor graphs follow the same pattern established in points a narrow temperature band consistent with the imposed wall heat flux, and a sharp, log-scale rise in particle concentration confined to the critical zone. The temperature graph at the highest heat transfer coefficient area shows in Figure 11. Therefore, the DPM concentration graph at the highest heat transfer coefficient area can be seen in Figure 12.

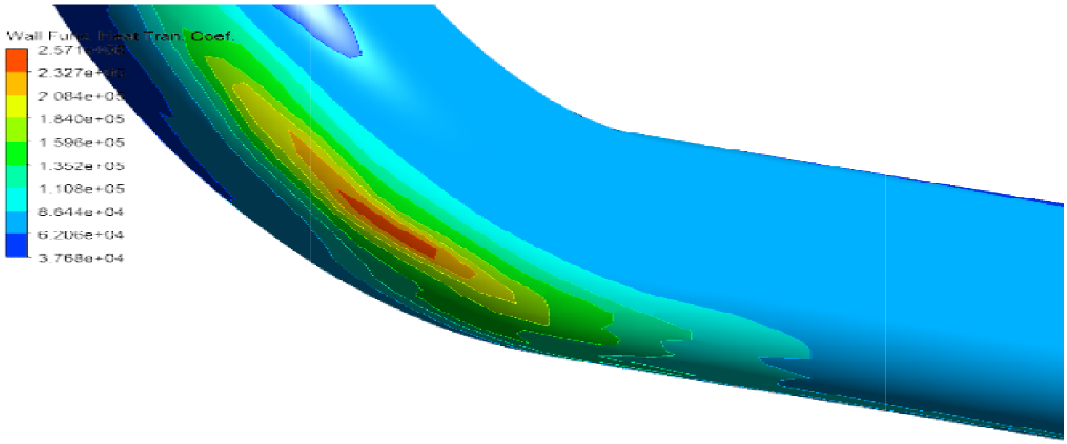

Figure 9: The highest heat transfer coefficient area

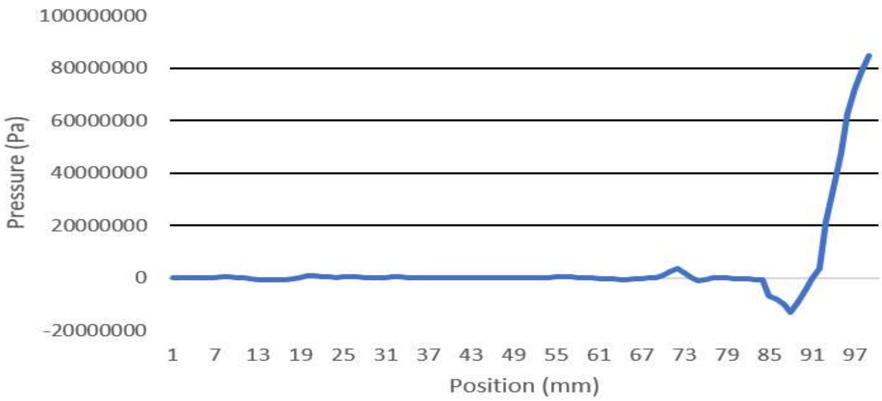

Figure 10: pressure graph at the highest heat transfer coefficient area

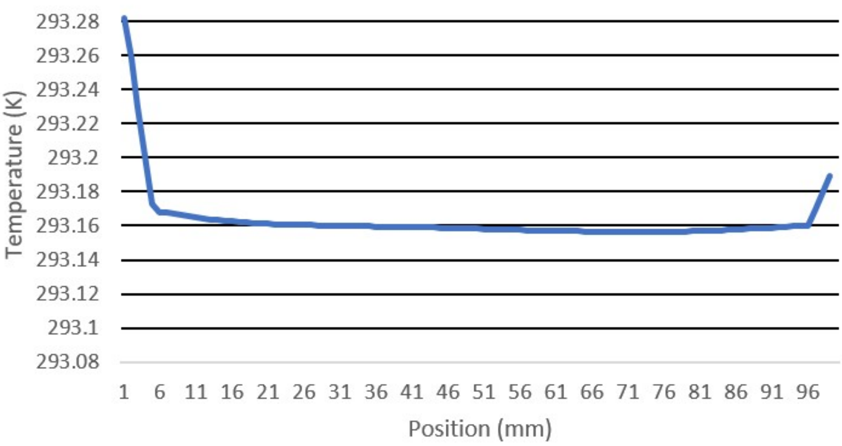

Figure 11: Temperature graph at the highest heat transfer coefficient area

JOMAse | Received: 20 March 2026 | Accepted: 30-March-2026 | [(70) 1: 100-107]
Published by International Society of Ocean, Mechanical and Aerospace Scientists and Engineers, www.isomase.org., ISSN: 2354-7065 & e-ISSN: 2527-6085

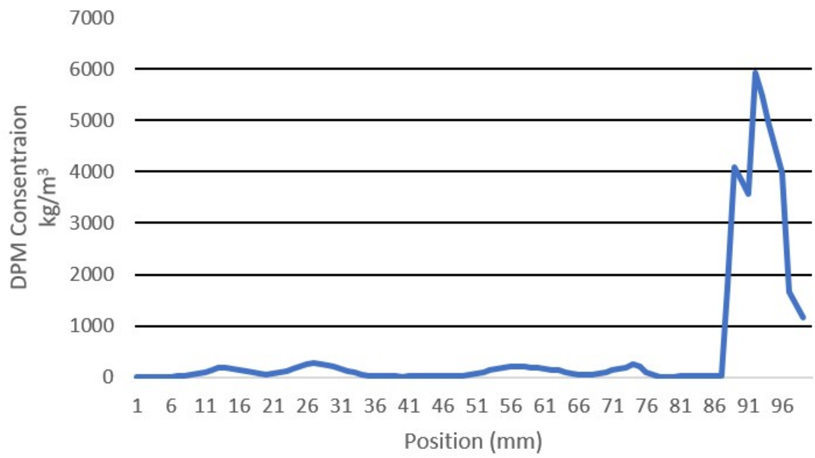

Figure 12: The DPM concentration graph at the highest heat transfer coefficient area

4. CONCLUSION

This study examined how bend-induced flow behavior in a 180° U-bend alters the convective heat transfer coefficient of Al_2O_3/water nanofluid at the highest Reynolds number investigated. The results show that the known enhancement mechanisms increased effective thermal conductivity, Brownian motion, changes in viscosity and boundary layer thickness, and particle-fluid interaction do not act uniformly once the fluid passes through the curved bend, but are instead redistributed circumferentially around the pipe. At the outer wall, centrifugal force drives the high-momentum core flow directly into the surface, producing a sharp local rise in the heat transfer coefficient that coincides with increased nanoparticle migration toward that wall confirming that the bend locally concentrates the effective-conductivity and particle-interaction mechanisms at this location. At the inner wall, the same centrifugal effect works in reverse, pulling flow away from the surface and yielding a consistently lower heat transfer coefficient. The side walls, shaped mainly by the tangential motion of the paired Dean vortices, show a more moderate and symmetric response between these two extremes, representing a distinct pattern rather than a simple blend of the other two. Overall, these findings confirm that U-bend geometry does not merely preserve straight-pipe nanofluid enhancement mechanisms it geometrically redistributes them, concentrating enhancement at the outer wall, suppressing it at the inner wall, and moderating it at the side walls. This behavior provides the basis for practical design guidance on heated-surface placement in U-bend heat exchangers using nanofluids.

5. REFERENCES

[1] Zeitoun, O. & Ali, M. (2012). Nanofluid impingement jet heat transfer. *Nanoscale Research Letters*, *7*(1), 139.

[2] Ahmed, Z., Al-Mussawi, W., Ghodratallah, P., Sadeq, A. M., Hussein, S. A., Rajab, H. & Louhichi, B. (2025). Numerical analysis of performance enhancement in a shell and double-coil heat exchanger using three passive flow and heat transfer methods. *The European Physical Journal Plus*, *140*(6), 567.

[3] Deeb, R. (2023). New correlations for predicting convective heat transfer of single and multi-row heat exchangers employing staggered drop-shaped tubes. *International Journal of Heat and Mass Transfer*, *202*, 123689.

[4] Ünverdi, M. (2022). Prediction of heat transfer coefficient and friction factor of mini channel shell and tube heat exchanger using numerical analysis and experimental validation. *International Journal of Thermal Sciences*, *171*, 107182.

[5] Alami, A. H., Ramadan, M., Tawalbeh, M., Haridy, S., Al Abdulla, S., Aljaghoub, H., ... & Olabi, A. G. (2023). A critical insight on nanofluids for heat transfer enhancement. *Scientific Reports*, *13*(1), 15303.

[6] Sundar, L. S., Kumar, N. R., Addis, B. M., Bhramara, P., Singh, M. K. & Sousa, A. C. (2019). Heat transfer and effectiveness experimentally-based analysis of wire coil with core-rod inserted in Fe3O4/water nanofluid flow in a double pipe U-bend heat exchanger. *International Journal of Heat and Mass Transfer*, *134*, 405-419.

[7] Barai, R., Kumar, D. & Wankhade, A. (2021). Heat transfer performance of nanofluids in heat exchanger: a review. *Journal of Thermal Engineering*, *9*(1), 86-106.

[8] Ukueje, W. E., Abam, F. I. & Obi, A. (2022). A perspective review on thermal conductivity of hybrid nanofluids and their application in automobile radiator cooling. *Journal of Nanotechnology*, *2022*(1), 2187932.

[9] Tao, Q., Zhong, F., Deng, Y., Wang, Y. & Su, C. (2023). A review of nanofluids as coolants for thermal management systems in fuel cell vehicles. *Nanomaterials*, *13*(21), 2861.

[10] Thesiya, D., Patel, H. & Patange, G. S. (2023). A comprehensive review electronic cooling: a nanomaterial perspective. *International Journal of Thermofluids*, *19*, 100382.

[11] Pak, B. C. & Cho, Y. I. (1998). Hydrodynamic and heat transfer study of dispersed fluids with submicron metallic oxide particles. *Experimental Heat Transfer an International Journal*, *11*(2), 151-170, doi: 10.1080/08916159808946559.

[12] Gabir, M. M., Albayati, I. M., Hatami, M. & Alkhafaji, D. (2024). An experimental investigation of the

convective heat transfer augmentation in U-bend double pipe heat exchanger using water-MgO-Cmc fluid. *Scientific Reports*, *14*(1), 12442, doi: 10.1038/s41598-024-63043-6.

[13] Clarke, R. & Finn, D. (2008). Numerical investigation of the influence of heat exchanger U-bends on temperature profile and heat transfer of secondary working fluids. *The 5th European Thermal-Sciences Conference, Eindhoven, the Netherlands*, 18-22 May 2008.

[14] Rao, V. N. & Sankar, B. R. (2017). CFD analysis of CuO/water nanofluid flow in a double pipe U-Bend heat exchanger. *International Journal of Dynamic of Fluid*, *13*(1), 137-152..

[15] Alguacil, F. J. & Alonso, M. (2024). The motion of Brownian particles suspended in a non-uniform fluid flow. *Journal of Aerosol Science*, *179*, 106382.

[16] Bacha, H. B., Ullah, N., Hamid, A. & Shah, N. A. (2024). A comprehensive review on nanofluids: Synthesis, cutting-edge applications, and future prospects. *International Journal of Thermofluids*, *22*, 100595, doi: 10.1016/j.ijft.2024.100595.

[17] Cengel, Y. A., Klein, S. & Beckman, W. (1998). *Heat Transfer: A Practical Approach* (Vol. 141). Boston: WBC McGraw-Hill.

[18] Schlichting, H. & Gersten, K. (2016). *Boundary-layer theory*. Springer Berlin Heidelberg, doi: 10.1007/978-3-662-52919-5.

[19] Chassagne, F., Barbour, M. C., Chivukula, V. K., Machicoane, N., Kim, L. J., Levitt, M. R. & Aliseda, A. (2021). The effect of Dean, Reynolds and Womersley numbers on the flow in a spherical cavity on a curved round pipe. Part 1. Fluid mechanics in the cavity as a canonical flow representing intracranial aneurysms. *Journal of Fluid Mechanics*, *915*, doi: 10.1017/jfm.2020.1114.